Disruption of Helix-Capping Residues 671 and 674 Reveals a Role in HIV-1 Entry for a Specialized Hinge Segment of the Membrane Proximal External Region of gp41

Zhen-Yu J. Sun[1], Yuxing Cheng[2], Mikyung Kim[2,3], Likai Song[4], Jaewon Choi[2], Ulrich J. Kudahl[5], Vladimir Brusic[3,5], Barnali Chowdhury[4], Lu Yu[4], Michael S. Seaman[6], Gaëtan Bellot[1,7,8], William M. Shih[1,7,8], Gerhard Wagner[1] and Ellis L. Reinherz[2,3]

*1 - **Department of Biological Chemistry and Molecular Pharmacology,** Harvard Medical School, Boston, MA 02115, USA*
*2 - **Laboratory of Immunobiology and Department of Medical Oncology,** Dana-Farber Cancer Institute, Boston, MA 02115, USA*
*3 - **Department of Medicine,** Harvard Medical School, Boston, MA 02115, USA*
*4 - **National High Magnetic Field Laboratory,** Florida State University, Tallahassee, FL 32310, USA*
*5 - **Cancer Vaccine Center and Department of Medical Oncology,** Dana-Farber Cancer Institute, Boston, MA 02115, USA*
*6 - **Department of Medicine,** Beth Israel Deaconess Medical Center, Boston, MA 02115, USA*
*7 - **Department of Cancer Biology,** Dana-Farber Cancer Institute, Boston, MA 02115, USA*
*8 - **Wyss Institute for Biologically Inspired Engineering at Harvard,** Boston, MA 02115, USA*

***Correspondence to Ellis L. Reinherz:** Laboratory of Immunobiology and Department of Medical Oncology, Dana-Farber Cancer Institute, Boston, MA 02115, USA. Ellis_Reinherz@dfci.harvard.edu*
http://dx.doi.org/10.1016/j.jmb.2013.09.030
Edited by E. O. Freed

Abstract

HIV-1 (*h*uman *i*mmunodeficiency *v*irus type *1*) uses its trimeric gp160 envelope (Env) protein consisting of non-covalently associated gp120 and gp41 subunits to mediate entry into human T lymphocytes. A facile virus fusion mechanism compensates for the sparse Env copy number observed on viral particles and includes a 22-amino-acid, lentivirus-specific adaptation at the gp41 base (amino acid residues 662–683), termed the membrane proximal external region (MPER). We show by NMR and EPR that the MPER consists of a structurally conserved pair of viral lipid-immersed helices separated by a hinge with tandem joints that can be locked by capping residues between helices. This design fosters efficient HIV-1 fusion via interconverting structures while, at the same time, affording immune escape. Disruption of both joints by double alanine mutations at Env positions 671 and 674 (AA) results in attenuation of Env-mediated cell–cell fusion and hemifusion, as well as viral infectivity mediated by both CD4-dependent and CD4-independent viruses. The potential mechanism of disruption was revealed by structural analysis of MPER conformational changes induced by AA mutation. A deeper acyl chain-buried MPER middle section and the elimination of cross-hinge rigid-body motion almost certainly impede requisite structural rearrangements during the fusion process, explaining the absence of MPER AA variants among all known naturally occurring HIV-1 viral sequences. Furthermore, those broadly neutralization antibodies directed against the HIV-1 MPER exploit the tandem joint architecture involving helix capping, thereby disrupting hinge function.

Introduction

Lentiviruses such as HIV-1 (*h*uman *i*mmunodeficiency *v*irus type *1*), the causative agent of acquired immunodeficiency syndrome (AIDS), are encapsulated in a membrane derived from the infected host cell as virus buds (reviewed in Refs. [1] and [2]). A trimeric Env gp160 spike consisting of three pairs of non-covalently associated gp120 and gp41 subunits is the only viral protein on the HIV-1 membrane. The Env gp120 mediates attachment and entry into human $CD4^+$ T lymphocytes upon binding its primary cellular receptor CD4 and CCR5 or CXCR4 co-receptor. Viral infectivity is dependent on membrane fusion between

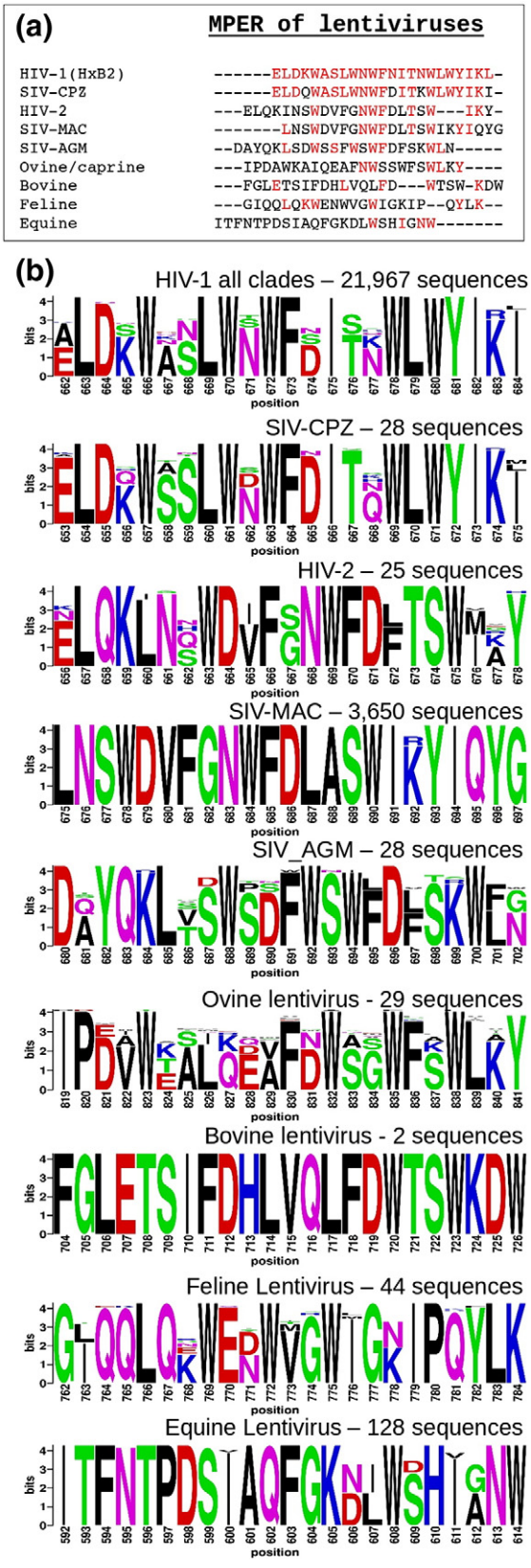

HIV-1 and the host cell through formation of a gp41 six-helix-bundle complex [3–5]. The efficiency of this mechanism is especially critical, given fewer than 12 copies of Env clustered on each viral particle [6].

The membrane proximal external region (MPER) is a tryptophan-rich segment located at the base of the gp41 subunit and appears to destabilize the viral membrane during the fusion process [7,8]. Deletion of the HIV-1 MPER, or concurrent mutation of three conserved tryptophan residues on its N-terminal helix to alanines, abolishes membrane fusion activity [9,10]. However, the presence of these conserved tryptophans alone is not sufficient to support the viral fusion activity [8]. Other MPER residues, even the exposed, primarily hydrophilic ones, may also be involved despite sequence variability therein. Previously, we solved the solution structure of a clade B HxB2 strain MPER peptide in detergent micelle with an unusual helix–hinge–helix motif [11]. Interestingly, the central hinge region is the target of several broadly neutralizing antibodies (BNAbs), including 4E10, 10E8 and Z13e1 [12–14]. Here, we provide detailed structural and functional results on this specialized hinge region relating to its potentially important role during the intermediate stages of the HIV membrane fusion process.

Results and Discussion

MPER sequence conservation and limited variability

Bioinformatics studies show that, while considerably conserved within each lentivirus group, the MPER sequences from HIV-1 and its ancestor SIV-CPZ (chimpanzee) are distinctive from those of HIV-2 and their related SIV-MAC (macaque) and SIV-AGM (African green monkey) sequences and are distant from non-primate lentiviruses (Fig. 1). As shown in Figs. 1b and 2a, the HIV-1 MPER is highly conserved across different clades. Structurally, the clade B HxB2 MPER peptide in dodecyl-phosphocholine (DPC) detergent micelle shows a helix–hinge–helix motif dictated by the segment's unique amphipathic pattern (Fig. 2b), with the membrane-buried residues mostly conserved and solvent-exposed residues relatively

Fig. 1. Comparison of MPER segments from nine groups of lentiviruses. The lentiviral segments, 23 amino acid long, N-terminal to their respective annotated transmembrane helices were extracted from SwissProt Database. (a) Sequence alignment with colored residues being identical with the reference sequence (HIV-1 HxB2). (b) Logos showing conservation within each of the nine lentivirus groups. The extremely conserved 3650 SIV sequences from rhesus macaque (SIV-MAC) is a result of infection in research primate centers.

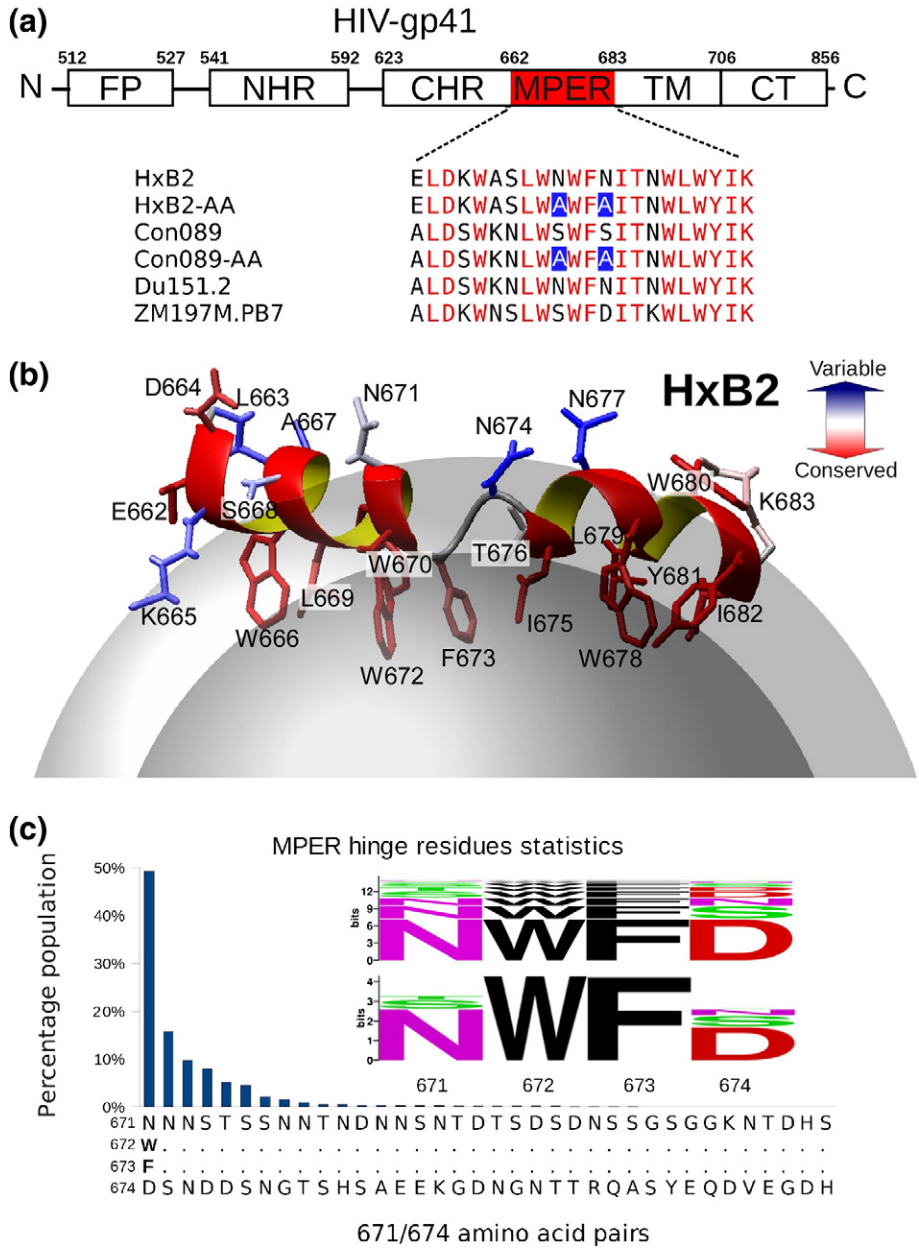

Fig. 2. Sequence conservation and variation of HIV-1 MPER. (a) Amino acid sequences of MPER peptides used for structural studies, with conserved residues colored red. (b) HxB2 MPER structure in a DPC detergent micelle with conserved and variable residues colored according to the scale shown. (c) Population of amino acid combinations at the 671 and 674 residue positions at the central hinge region, with BlockLogo sequence conservation diagram of the 671–674 segment shown as an inset at the top and conventional Shannon entropy representation of individual amino acid position variability at the bottom.

more variable. This pattern is prominent at the central hinge region, where the two key epitope residues for BNAb 4E10 and 10E8, W672 and F673, are essentially invariant and buried in the membrane, while the exposed N671 and N/D674, key epitope residues for Z13e1, manifest significant sequence variability (Fig. 2b and c). Using the "Motif-finder" software [15] and Los Alamos HIV database, we have identified all 36 amino acid residue combinations at the 671 and 674 positions. This is a surprisingly small number taken from among 21,967 HIV-1 strain sequences across all major clades (Fig. 2c), and the residue types are dominated by asparagine, aspartate, serine and threonine (NDST set) (Table 1).

Table 1. Sequence (singly) variability of residues 671 and 674 in all HIV-1 strains.

Rank	Amino acid	Frequency (%)	Accumulated frequency (%)	Sequences
Residue 671				
1	N	78.42	78.42	17,226
2	S	14.91	93.33	3276
3	T	5.99	99.32	1316
4	D	0.64	99.96	140
5	X	0.02	99.98	4
6	G	0.01	99.99	3
7	H	0.00	100.00	1
8	K	0.00	100.00	1
Residue 674				
1	D	62.41	62.41	13,709
2	S	21.06	83.47	4627
3	N	12.05	95.52	2646
4	G	1.81	97.33	398
5	T	1.03	98.36	226
6	E	0.51	98.86	111
7	H	0.51	99.37	111
8	A	0.33	99.70	73
9	K	0.23	99.93	50
10	X	0.04	99.96	8
11	Q	0.01	99.98	3
12	R	0.01	99.99	3
13	Y	0.00	100.00	1
14	V	0.00	100.00	1

More than 96.5% of the residue pairs (doubly) in the MPER of 21,967 HIV-1 strains are exclusively from the NSTD set (shaded); all but two pairs had at least one residue from this set.

Hinge mutations impacting HIV-1 viral infectivity

To determine the functional role of the MPER hinge region and investigate the impact of sequence variations at residues 671 and/or 674 on virus entry, we produced viruses pseudotyped with MPER mutants by co-transfection of 293T cells with an Env-deficient HIV-1 (pSG3ΔEnv) backbone and an Env-expressing plasmid. The infectivity of pseudotyped viruses was then determined in TZM-bl ($CD4^+CXCR4^+CCR5^+$) cells and read out as RLU (*r*elative *l*ight *u*nits). The mutations of the HIV-1 Con089 clade C strain were generated by changing serine S671 and S674 residues (SS) in the wild-type (WT) sequence to NN, NG, NA and AA, respectively. Likewise, T671 and D674 (TD) of the WT Env from the clade B CAAN strain were mutated to DD, ND and SD. All except the AA mutations represent combinations found in naturally occurring HIV strains (Fig. 2c).

Figure 3a shows that changing the residue in the WT sequence at these two amino acid positions to commonly represented residues (such as N, D, S or T) was well tolerated by the mutant pseudoviruses. In contrast, viral infectivity was reduced 6-fold for the non-native AA mutation. Serial dilutions of Env-pseudotyped virus stocks with AA mutants from both Con089 and HxB2 strains further confirmed the effect of hinge region AA mutation on virus infectivity in TZM-bl cells (Fig. 3b). The block to virus infectivity was greater with the AA mutation in the CXCR4-dependent strain HxB2 (reduction by more than 10-fold) but nonetheless significant (6- to 7-fold reduction) in both CCR5-dependent Con089 (Fig. 3b) and PB7 strains (data not shown), indicating that the attenuation of viral infectivity was independent of co-receptor usage. Note the $\log_{10}$ scale used for both *x*- and *y*-axes.

One possible explanation for the reduced viral infectivity might be linked to structural changes within the gp120/gp41 trimer induced by the AA mutation in the MPER impacting receptor binding. This possibility was excluded by examining an AA mutant of the CD4-independent chimeric strain, ADA/Hx(197) [16]. ADA/Hx-AA mutant resulted in a significantly decreased capacity to infect both $CD4^+$ TZM-bl (Fig. 3c, top) and $CD4^-$ Cf2Th/Syn CCR5 (Fig. 3c, bottom) cells (~70-fold reduction from WT). Thus, it appears that the AA mutation effect is significantly more pronounced in a CD4-independent strain. In addition, no effects of this AA mutation on the efficiency of gp160 envelope protein precursor processing to gp120 or expression level were observed on these pseudoviruses (Fig. 3c, inset).

Double alanine MPER mutant affects viral membrane fusion

We next examined the effect of AA mutation on gp41-mediated fusion by a fluorescence cell–cell fusion assay. Env-expressing 293T effector cells stained with cytoplasmic dye Calcein-AM (green) were co-cultured with 3T3.CD4.CCR5 target cells stained with CellTracker orange CMTMR (red), and the exchange of cytoplasmic dyes between effector and target cells was monitored by fluorescence microscopy. The JRFL-AA mutant exhibited both reduced numbers and sizes of syncytia (appearing orange/yellow) at 4-h co-culture compared to WT (Fig. 4a, top row), at levels comparable to the JRFL cleavage (–) negative control. A similar observation was made with ADA-AA compared to ADA-WT at 4 h. However, using bright field illumination at 24 h, while syncytia in JRFL-AA were significantly smaller than JFRL-WT syncytia (Fig. 4a, bottom row), the ADA-WT and ADA-AA syncytia were more comparable (data not shown), arguing that MPER function may be critical for early fusion events. This possibility was confirmed in subsequent lipid mixing/hemifusion assays below.

To quantitatively assess fusion efficiency, we utilized TZM-bl cells expressing luciferase under the control of the HIV long terminal repeat promoter responsive to HIV Tat as targets. The results confirmed impairment of cell–cell fusion by AA mutation in the MPER of JRFL and ADA strains. Fusion efficiency was reduced by ~50% in the first 6 h in both strains (Fig. 4b). The reduced fusion

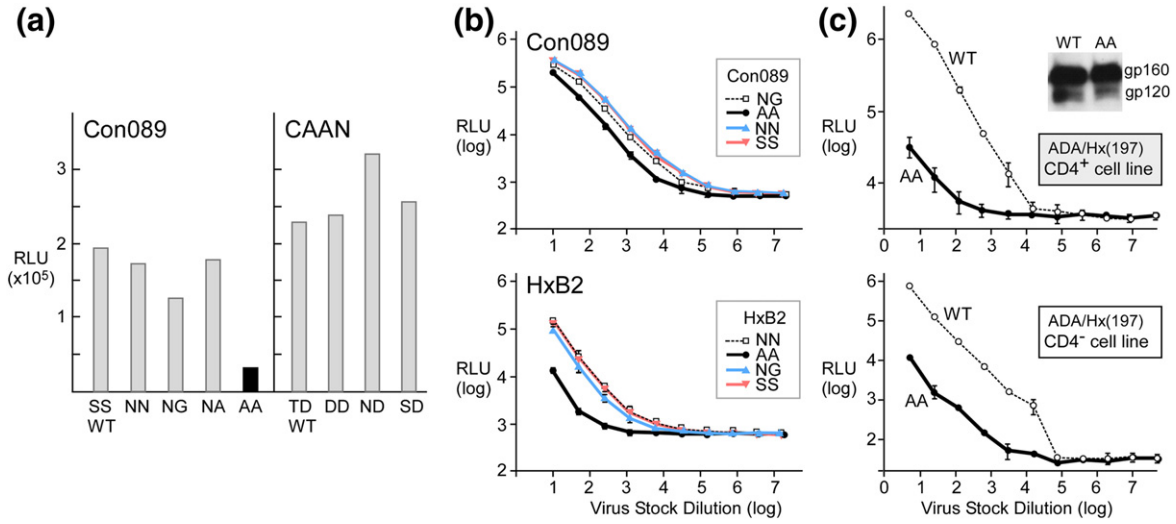

Fig. 3. HIV-1 pseudovirus infectivity affected by AA mutations. (a) Infectivity of pseudoviruses harboring the Env mutations at positions 671 and 674. Comparable number of viral particles were used as determined by p24 Elisa. (b) Titration (log_{10}) of Con089 and HxB2 Env WT or mutant pseudoviruses on TZM-bl cells. Mean and standard deviation of each dilution is shown. (c) Dose-dependent infectivity of CD4-independent ADA/Hx(197) pseudoviruses on $CD4^+$ $CCR5^+$ TZM-bl cells and $CD4^-$ Cf2Th/Syn CCR5 cells. The inset shows anti-gp120 mAb Western-blot of ADA/Hx(197) Env from pseudovirus.

efficiency was independent of surface expression level and envelope protein precursor processing. To further study the fusion block at the early lipid mixing/hemifusion phase, we used membrane probes in an experiment where DiO-labeled Env-293T cells (green) were co-cultured with DiI-labeled 3T3.CD4.CCR5 (red) target cells for 2 h. Figure 4c shows DiI-labeled individual cells associated with DiO-labeled effector cells and also transfected with a cleavage site defective Env as a negative control. Whereas extensive dye redistribution with numerous co-localization events (spotting on cell surfaces) was observed for JRFL-WT, reduced co-localization for JRFL-AA was observed which indicated blocking of lipid mixing, similar to the JRFL cleavage (–) negative control. Using flow cytometry analysis to quantity the double fluorescence cells, we observed hemifusion to be reduced by ~50% for the JRFL-AA compared to JRFL-WT (Fig. 4d). Collectively, these findings document a selective detrimental effect of MPER AA mutation on viral fusion and infection.

MPER helix–hinge–helix motif is a common feature in both clade B and clade C HIV-1 strains

To understand the impact of hinge residue variation at the 671 and 674 positions on MPER conformation, we carried out NMR and EPR spectroscopy studies on several native and mutant MPER peptides (Fig. 2a). The solution structures of three clade C peptides, Con089, Du151.2 and ZM197M.PB7 in DPC micelles (Fig. 5a and Table 2), adopt the same helix–hinge–helix motif as the previously solved clade B HxB2 peptide [11]. These new peptides used in NMR studies all contain five additional native N-terminal residues from the gp41 CHR (*C*-terminal *h*eptad *r*epeat), EQELL for clade B and EKDLL for clade C strains. As represented by the clade C Con089 peptide in DPC detergent micelles shown in Fig. 5b, the N-terminal extension forms a fishhook-like turn stabilized by two conserved leucine residues L660 and L661 inserted into the membrane phase, as well as a hydrogen bond between the side-chain amide of W666 and the backbone carbonyl of L661. This N-terminal extension from CHR is highly mobile and apparently has little effect on the rest of the peptide structure.

The statistical results of NMR structural calculations are summarized in Table 2, including residual dipolar coupling (RDC) constants measured using a DNA nanotube detergent-resistant alignment medium [17]. The RDC values obtained from multiple JNH, JNCO, JCOCA and JCAHA quantitative J experiments are incompatible with a single alignment tensor for the entire MPER peptide. However, the N-terminal and C-terminal helical segments of these MPER peptides can be fitted with two independent alignment tensors, consistent with the flexibility afforded by the central hinge (Fig. 5a). The highly mobile MPER N-terminal region (657–665) and the C-terminal residue (683), as well as the central hinge region (672–673), are excluded from RDC data analysis. The similarity of RDC alignment tensors between Con089 and Du151.2 confirmed

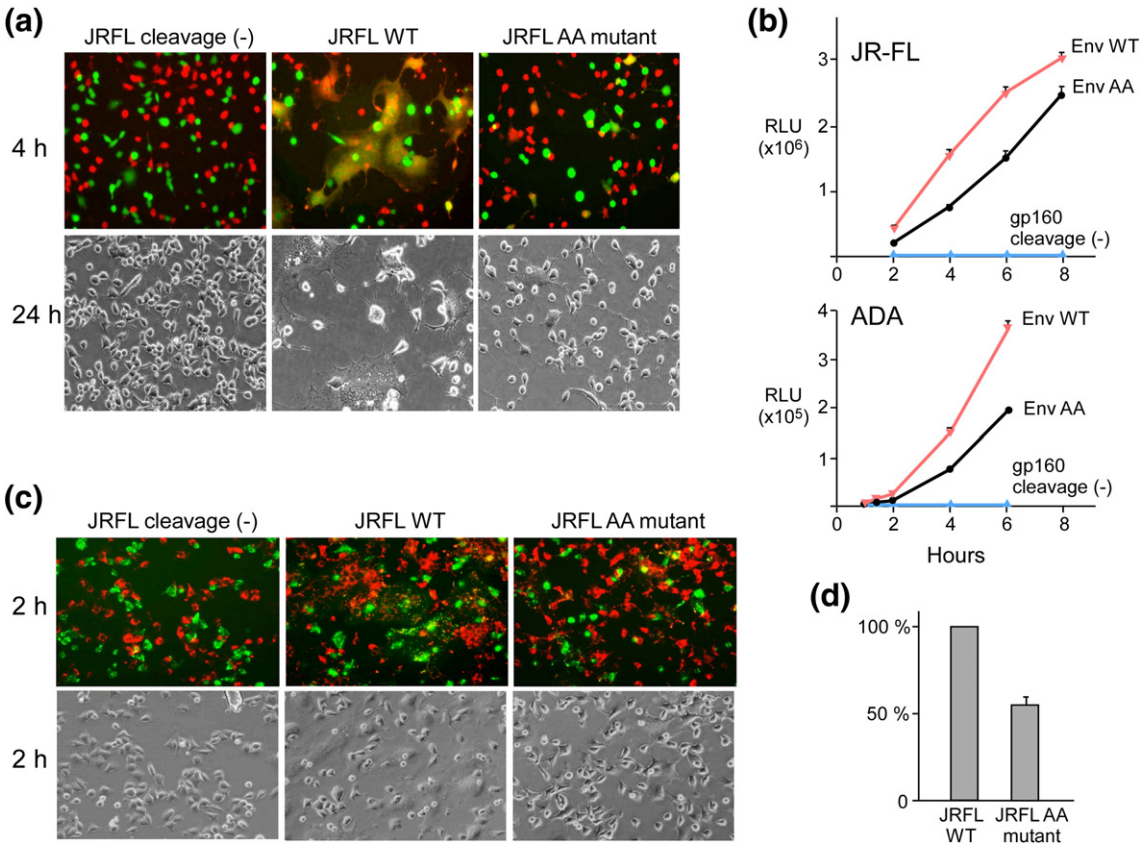

Fig. 4. Env-mediated fusion impaired by AA mutations. (a) Qualitative microscopy analysis of cell–cell fusion. Content mixing of Env-expressing 293T effector cells with 3T3.CD4.CCR5 target cells. The top row shows the overlay of fluorescence images after co-incubation of 293T cells (green, Calcein) with 3T3.CD4.CCR5 cells (red, CMTMR) at 37 °C for 2 h. The bottom row shows representative bright field images collected 24 h after co-incubation at 37 °C. (b) Fusion kinetics of JRFL (top) or ADA (bottom) Env-expressing 293T cells with TZM-bl cells containing a Tat-driven luciferase reporter. (c) Hemifusion identified by lipid mixing between DiO-labeled 293T cells (green) and DiI-labeled 3T3.CD4.CCR5 cells (red). The top row shows the overlay of fluorescence images collected 2 h after co-incubation at 37 °C. The bottom row shows the corresponding bright field images. (d) Quantitative lipid mixing efficiency of JRFL-AA relative to WT. Flow cytometric analysis of lipid-dye transfer between DiO-labeled 293T cells and DiD-labeled TZM-bl cells were conducted. The percentage of lipid mixing activities were determined following the subtraction of background dye redistribution between empty vector-transfected effector and target cells, normalized to that of WT (100%) in three independent experiments.

that the two peptides have very similar orientations as they differ only by two residues at 671 and 674 positions (Figs. 2a and 5a). RDC values for the clade C peptide ZM197M.PB7 are rather different due to its distinctive charged residue distribution (Fig. 2a), resulting in different alignment tensor in the DNA nanotube alignment medium.

Distinctive conformation of MPER AA mutant peptide

The structure of HxB2-AA peptide does not have the generally L-shaped bend as observed with the other MPER peptides (Fig. 5a). In addition, the N-terminal helix is extended by one residue to F673, while the C-terminal helix is shortened by two residues at the N-terminal end (Fig. 5c). This distorts the original central hinge region, resulting in an elongated and partially unstructured linker region between residues 674 and 677. The alanine residues at 671 and 674 positions are not exposed to the solvent as is typical for other MPER peptides (Fig. 5b and c).

Measured JNH RDC values between HxB2 WT and HxB2-AA mutant peptides in DPC micelles show a weaker correlation with a reduced R^2 value compared to that between Con089 and Du151.2 (Fig. 5d, left panels), which have similar orientations. This is despite the fact that each pair differs only at residue positions 671 and 674 by the change of asparagine to serine or alanine and maintains the same charged residue distribution (Fig. 2a). Thus, the RDC values from HxB2 and HxB2-AA mutant MPER peptides must diverge as a result of structural differences on the membrane surface, most noticeably near the

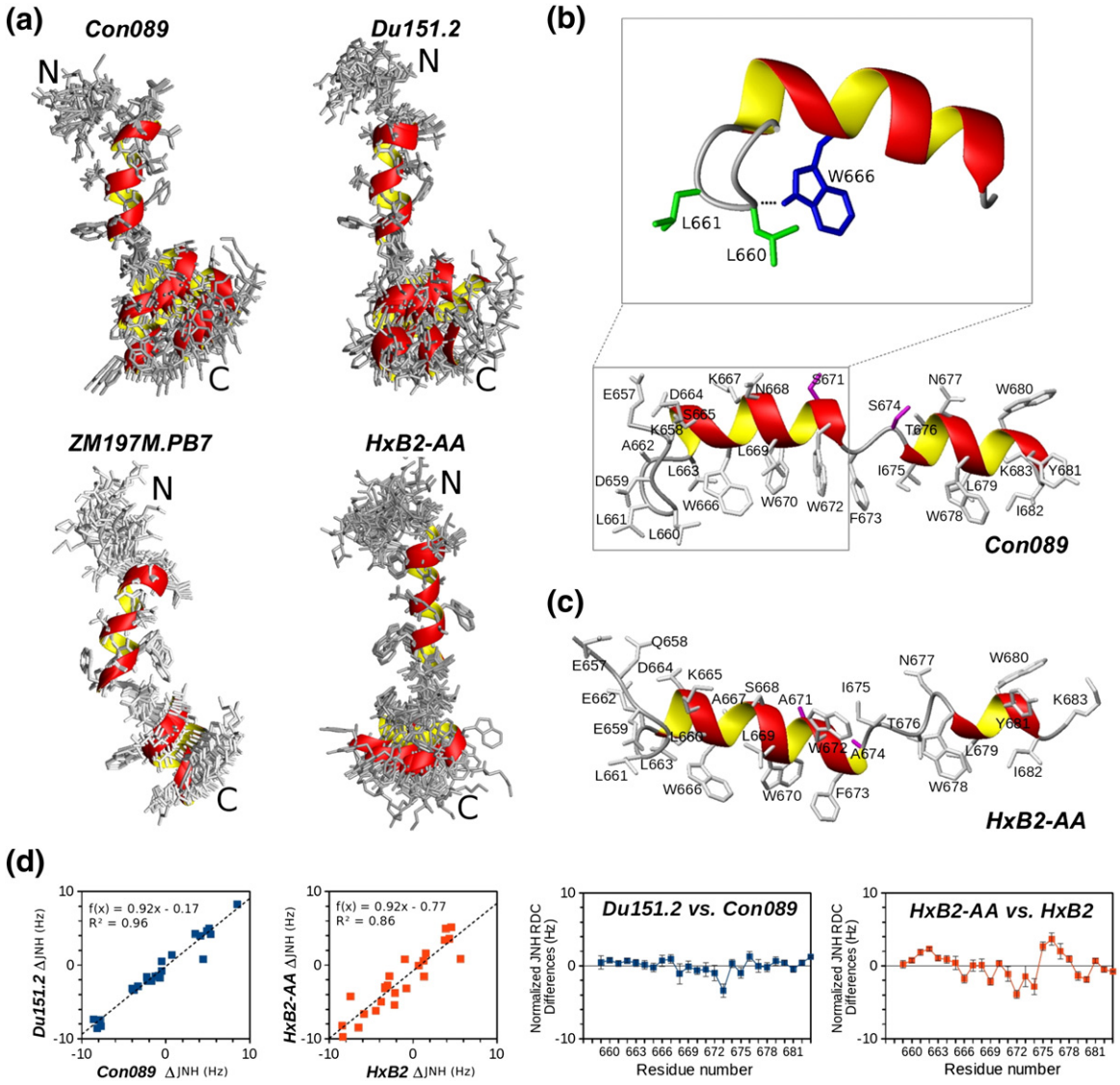

Fig. 5. Solution structures of MPER peptides. (a) NMR structure ensembles of Con089, Du151.2, ZM197M.PB7 and HxB2-AA MPER peptides in DPC detergent micelles, superimposed by their N-terminal helices (666–672). (b) The additional CHR residues at the N-terminal end of MPER, as represented here by the Con089 peptide in DPC micelles, all adopt a conserved beta turn stabilized by L661/L662 and W666. (c) Ribbon diagram of a representative HxB2-AA peptide with the side chains of alanine substituted residues colored pink. (d) The left panels show JNH RDC values with good correlation between Con089 and Du151.2 but weaker correlation between HxB2 and HxB2-AA. The right panels show difference in JNH RDC values (normalized according to fitted linear correlation parameters) between Con089 and Du151.2 and between HxB2 and HxB2-AA. The errors are derived from NMR amide peak position estimates.

distorted hinge regions (Fig. 5d, right panels). The same patterns are observed for other RDC types, but JNH RDC values shown here are more accurate and easiest to measure experimentally.

Atypical behavior of MPER AA mutant on membrane surface

EPR immersion depth measurements for the three clade C MPER peptides, Con089, Du151.2 and ZM197M.PB7, also showed comparable overall structure and membrane immersion in POPC:POPG (4:1 by weight) liposomes (Fig. 6a). Similar to HxB2 [11], the acyl chain-facing and aqueous-facing side chains judging by their immersion depths alternate every third or fourth sequence position from 666 to 673 and from 675 to 681, consistent with helical conformation. However, the immersion depth data are out of phase at residue position 674, supporting the helix–hinge–helix motif. Taken together, the helix–hinge–helix motif

Table 2. NMR statistics.

	Con089[a]	Du151.2	ZM197M.PB7	HxB2-AA[b]
Total NOE restraints	440	383	430	335
Intra-residue	145	138	175	159
Medium range (≤4)	286	233	251	170
Long range (>4)	9	12	4	6
Dihedral angle restraints	45	47	46	47
RDC restraints	60	58	55	50
Membrane depth restraints	14	15	15	16
Backbone ⟨RMSD⟩ to mean (Å)				
666–682	0.78	0.94	0.32	0.59
N-helix (666–672)	0.04	0.05	0.05	0.09[b]
C-helix (675–682)	0.06	0.32	0.06	0.08[b]
Ramachandran statistics (%)				
Most favored regions	81.2	76.8	83.6	78.8
Additionally allowed regions	18.4	21.6	16.4	21.2
Generously allowed regions	0.4	1.6	0	0
Disallowed regions	0	0	0	0
Alignment tensor				
Da (N-helix)	9.32 ± 0.11[a]	9.32 ± 0.04	4.51 ± 0.02	7.19 ± 0.06[b]
R (N-helix)	0.13 ± 0.01[a]	0.18 ± 0.01	0.38 ± 0.01	0.43 ± 0.01[b]
Da (C-helix)	4.74 ± 0.04[a]	4.12 ± 0.09	2.72 ± 0.03	4.98 ± 0.04[b]
R (C-helix)	0.53 ± 0.02[a]	0.41 ± 0.04	0.13 ± 0.01	0.31 ± 0.01[b]

[a] The alignment tensor parameters for Con089 shown above were obtained with JNH and JCAHA RDCs only. RDCs of JNCO and JCOCA were acquired with a second DNA sample that yield Da = 9.71 ± 0.04, R = 0.24 ± 0.01 for N-helix, and Da = 4.24 ± 0.03, R = 0.48 ± 0.01 for C-helix.

[b] The HxB2-AA ensemble has 10 accepted conformers selected from 30 calculated structures (20 for other peptides). The N- and C-helix regions for HxB2-AA are defined as 666–673 and 678–682, respectively.

in MPER is likely a conserved feature in all HIV-1 clades and potentially the ancestral SIV from chimpanzee (Fig. 1).

In contrast, EPR immersion depth measurements show an altered membrane immersion pattern for HxB2-AA mutant as compared to other MPER peptides (Fig. 6a). There are more residues buried in the aliphatic region and fewer residues with complete solvent exposure in the case of the HxB2-AA mutant. The depth pattern of Con089-AA mutant peptide was also an outlier (data not shown). Figure 6b shows the side views of the MPER peptides embedded in the membrane by incorporating EPR immersion depth restraints in the NMR structure calculations. The HxB2-AA mutant peptide has a deeply buried middle section, bending in a different orientation with respect to other native MPER peptides (Figs. 5a and 6b).

EPR double electron–electron resonance (DEER) spectra of singly spin-labeled HxB2-AA MPER peptides at residue position W670, W678, or Y681 show detectable spin–spin distances (<30 Å) consistent with peptide dimerization (Fig. 6c). NMR results also suggest that the HxB2-AA MPER mutant tends to aggregate at high concentrations, as the amide backbone peaks become broadened and some of them disappeared (Fig. 6d) even in DPC micelles. These changes were not observed for other native MPER peptides and can be attributed to the double substitution of asparagine at residue positions 671 and 674 by alanines and the associated increase in hydrophobicity.

Alternative N-capping of the MPER C-terminal helix

How does the double alanine substitution of MPER 671/674 hinge residues functionally impact HIV-1 infection during the early membrane fusion stages (Fig. 7a)? First, MPER hinge distortion and aggregation might alter gp41 trimer interface and indirectly induce structural change around the CD4 binding site in the pre-fusion state. However, this possibility cannot explain AA mutation effects on CD4-independent virus infectivity (Fig. 3c). Alternatively, the AA mutation might destabilize gp41 6-helix bundle-mediated membrane pore formation manifest in the post-fusion state. This is also unlikely given only minor contacts involving residues 671 and 674 in a six-helix-bundle structure including MPER segment [18]. Third, the AA mutant MPER could impede the assembling of the gp41 six-helix bundle during the fusion intermediate stages, hindering the kinetics of the early membrane fusion process (Fig. 7a) in agreement with our experimental findings and the structural implications discussed below.

Native MPER 671 and 674 position residues overwhelmingly belong to the NDST set (Table 1), a prominent feature for all HIV-1, HIV-2 and SIV

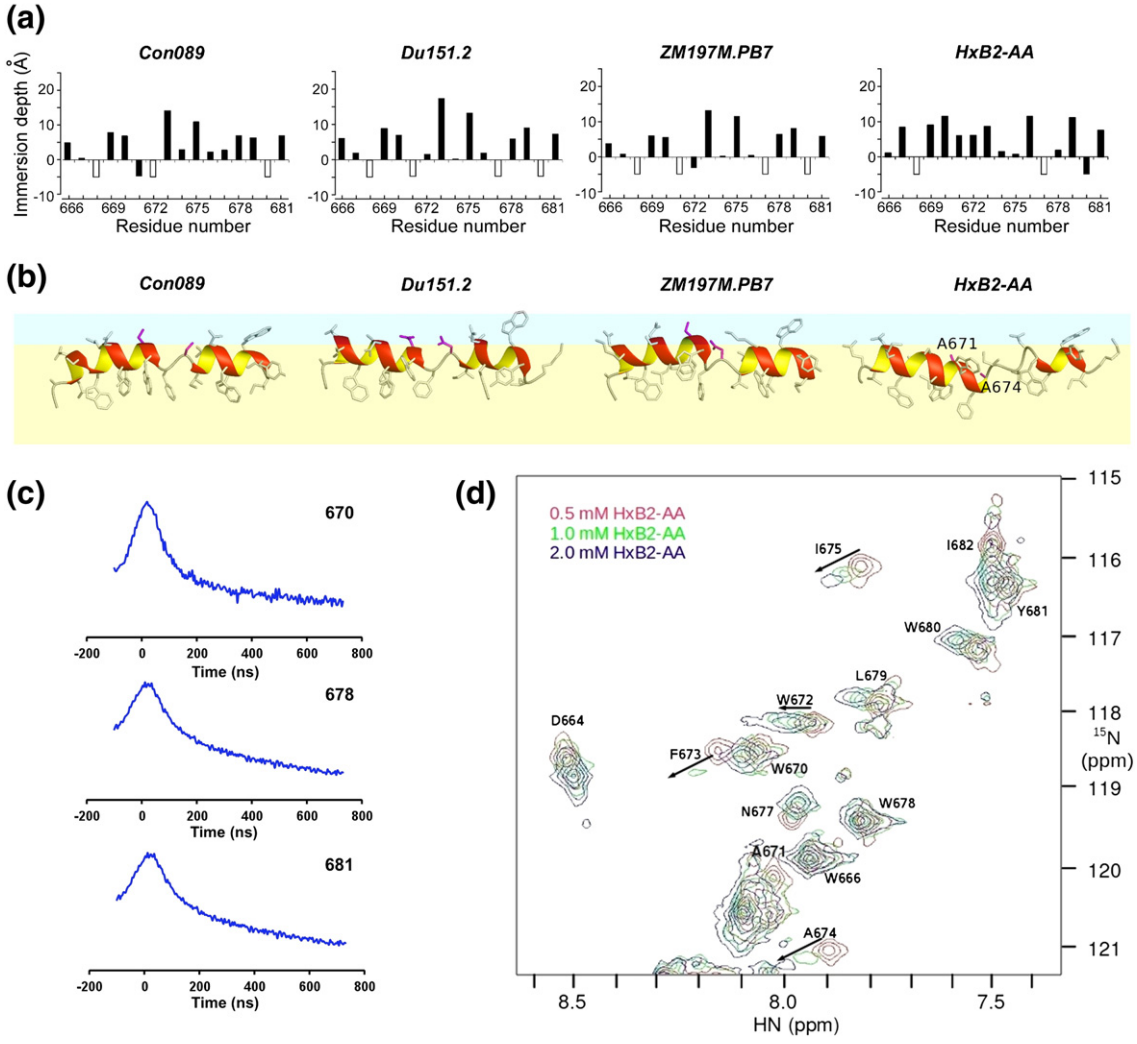

Fig. 6. Structural comparison with MPER AA mutant. (a) EPR membrane immersion depths of Con089, Du151.2, ZM197M.PB7 and HxB2-AA in liposomes. Depth values between −5 Å to 0 Å and larger than 0 Å correspond to lipid head-group region and acyl-chain region, respectively. The white-colored bars indicate complete exposure to aqueous phase (depth is less than −5 Å). (b) NMR structure models of representative Con089, Du151.2, ZM197M.PB7 and HxB2-AA peptides on the membrane surface. The lipid head-group and acyl-chain regions are shown in light blue and yellow, respectively. Residues 671 and 674 are colored pink. The N-terminal extended regions (657–661) are omitted for simplicity. (c) EPR DEER spectra of singly spin-labeled HxB2-AA MPER peptides at residue positions 670 (top), 678 (middle) and 681 (bottom) showing spin–spin correlation consistent with peptide dimerization. (d) NMR ^{15}N-heteronuclear single quantum coherence spectra of HxB2-AA MPER in DPC micelles, showing broadening and disappearance of some backbone amide peaks at higher peptide concentrations consistent with aggregation.

lentiviruses (Fig. 1). The asparagine, aspartate, serine and threonine residues are favored as helix N-cap residues by forming side chain-to-main chain hydrogen bonds to stabilize the N-terminal end of alpha helices [19,20]. This is consistent with the breaking of N- and C-terminal helices of the MPER to adopt a helix–hinge–helix motif. Figure 7b shows backbone dihedral angle predictions based on observed NMR chemical shifts that reveal the breakage of helices in the 2F5-bound MPER [21,22] [23] and the 4E10-bound MPER [24] at residue 671 and in the Z13e1-bound MPER [24] at residue 674. Helix breakage at residue 671 is also observed in the X-ray crystal structure of the 10E8-bound MPER [13]. Indeed, the side chains of MPER residues N671/D674 form hydrogen bonds to the backbone amides of the C-terminal helix residues in all of the aforementioned MPER-neutralizing antibody complexes (Fig. 7c). Similar helix breakage at residue 674 can also be observed for unbound Con089 MPER peptides in DPC micelles, but not for HxB2-AA (Fig. 7b).

Helix N-capping has been shown to regulate kinetics of light-induced conformational changes in a PYP PAS domain [25], to correlate with allosteric

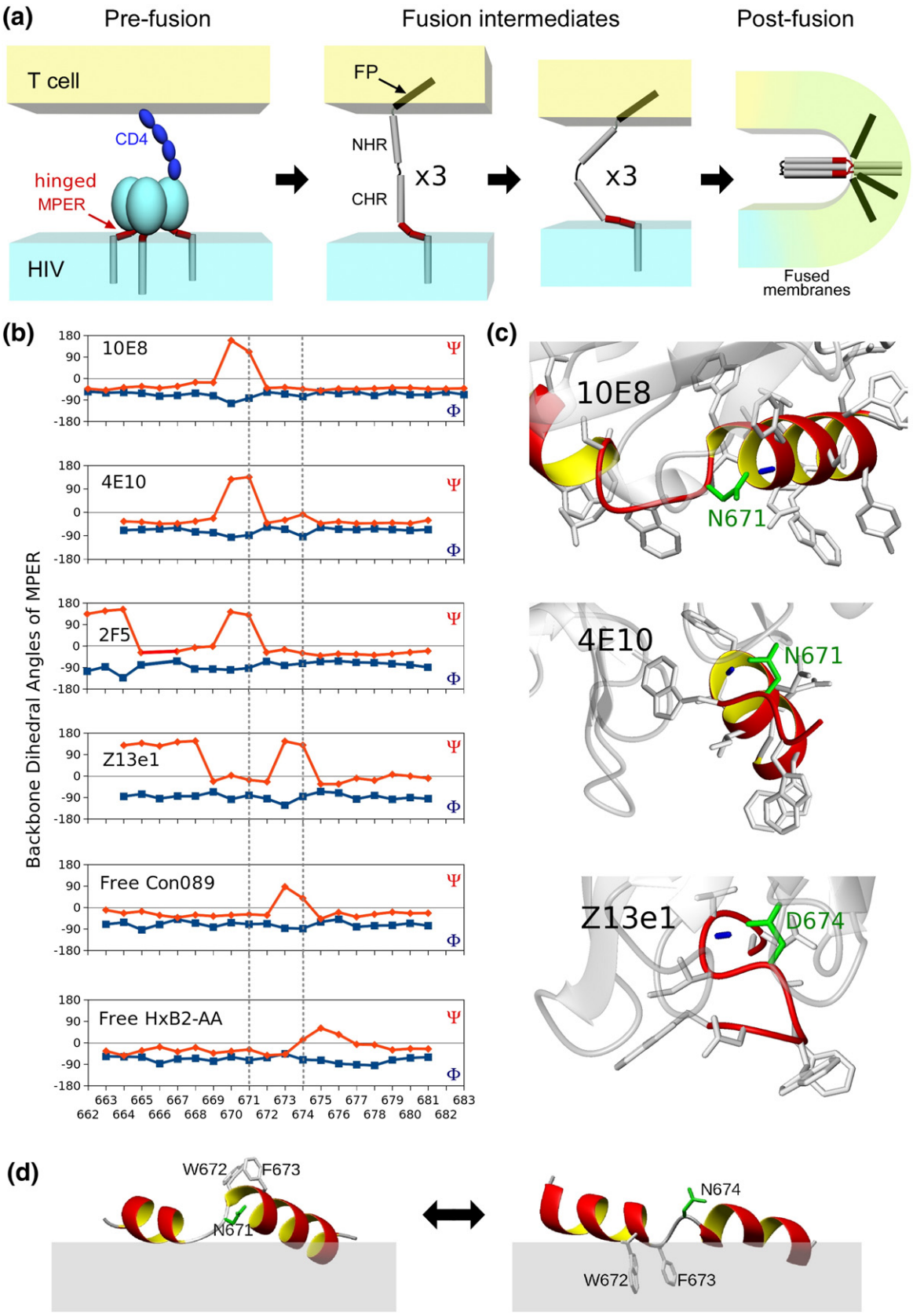
(a)
Pre-fusion
Fusion intermediates
Post-fusion
T cell
CD4
hinged
MPER
HIV
FP
NHR
CHR
x3
x3
Fused
membranes
(b)
Backbone Dihedral Angles of MPER
10E8
4E10
2F5
Z13e1
Free Con089
Free HxB2-AA
Ψ
Φ
180
90
0
-90
-180
662 663 664 665 666 667 668 669 670 671 672 673 674 675 676 677 678 679 680 681 682 683
(c)
10E8
N671
4E10
N671
Z13e1
D674
(d)
W672
F673
N671
N674
W672
F673

activation in a cAMP receptor via helix breakage [26] and to maintain continuous curvature on the surface of a retroviral capsid via an inter-domain hydrogen bond [27]. The first structural implication of our results is that the gp41 ectodomain could pivot in a rigid-body motion via the MPER central hinge region. The helix–hinge–helix motif, strengthened by the N-capped MPER C-terminal helix, could exert force on the lipid bilayer while, at the same time, adapting to membrane curvature during viral membrane fusion. Secondly, as shown in Fig. 7d, the orientations of the two central residues, W672 and F673, relative to the membrane in relation to the helical break at either 671 (left) or 674 (right) joint position are strikingly different. It appears that the formation of a "sliding" hinge region, facilitated by helix N-capping at a pair of tandem joint positions of the MPER (Fig. 7b), could potentially promote lipid mixing by allowing such "rotary" motion of bulky aromatic residues with respect to the viral membrane.

Since alanines have the highest helical propensity [28] but are unsuitable for capping a helix, double alanine mutations of MPER would disrupt the conserved helix–hinge–helix motif. Hence, in MPER-AA mutant, the extension of the N-terminal helix, deeper embedding in the membrane and inefficient C-terminal helix breaking, all contribute to reduced fusion activity and viral entry. In essence, the HIV-1 apparently incorporates a flexible and "fail-safe" tandem joint region, rationalizing why the double AA mutation in the MPER cannot exist in nature. However, by immobilizing the central hinge region, MPER-targeted BNAbs hinder HIV-1 fusion and infectivity.

Materials and Methods

Materials

Lipids, liposome preparation, synthetic peptide production with and without spin-labels and procedures for GB1-MPER fusion protein production in *Escherichia coli* were previously described [11,24]. NMR stable isotope labels and d38-DPC detergent was purchased from Cambridge Isotope Laboratories (Andover, MA). Env-expressing plasmids JRFL delCT(+) (cytoplasmic tail deletion with WT cleavage site), JRFL delCT(–) (mutated cleavage site) and Tat-expressing plasmid pcTAT were kindly provided by Dr. Richard T. Wyatt (The Scripps Research Institute). Env-expressing plasmids to make CD4-independent pseudoviruses ADA/Hx(197) were kindly provided by Dr. Joseph G. Sodroski (Dana-Farber Cancer Institute). Con089 Env plasmid was kindly provided by Drs. Bart Haynes (Duke University) and Ronald Swanstrom (University of North Carolina at Chapel Hill). 293T cells were purchased from American Type Culture Collection. TZM-bl cell, 3T3.CD4.CCR5 cell and $CD4^-$ Cf2Th/Syn CCR5 were obtained from the AIDS Research and Reference Reagent Program, National Institutes of Health.

Preparation of pseudoviruses

Single-round, recombinant HIV-1 viruses [Con089, CAAN, HxB2 and ADA/Hx(197)] were generated by transfection of 293T cells using an Env-deficient HIV-1 (pSG3ΔEnv) backbone and Env-expressing plasmid. Briefly, cells were seeded in 10-cm dish (approximately 3×10^6 cells per dish) and transfected the next day with pSG3ΔEnv and Env-expressing plasmid. Seventy-two hours after the transfection, virus-containing supernatants were collected, cleared of cell debris by low-speed centrifugation and filtered through 0.45-mm filters. To produce pseudoviruses that contain the luciferase gene to infect Cf2 Th/Syn CCR5 cell, we transfected 293T cells with the HIV-1 packaging plasmid pCMVDP1DenvpA, the firefly luciferase-expressing plasmid pHIvec2.luc and the plasmid expressing the HIV-1 Rev protein and the envelope protein. The amount of virus particles produced was determined using Alliance HIV-1 p24 antigen ELISA Kit (Perkin Elmer, Waltham, MA) per product manual. To prepare viruses pseudotyped with mutant Env protein, we created mutations by site-directed mutagenesis with QuikChange™ Site-Directed Mutagenesis Kit (Stratagene, Santa Clara, CA).

Virus infection

Target cells (10,000 cells per well) were seeded into all wells of a 96-well flat-bottom culture plate. Serial 5-fold dilutions for a total of 11 dilutions of stock pseudoviruses with comparable level of p24 were added into quadruplicate wells. We added 20 μg/ml DEAE-dextran to enhance virus infection. Target cells were then incubated at 37 °C for 48 h before the measurement of luminescence using Steady-Glo Luciferase assay system (Promega, Madison, WI).

293T cell transfection

Cell–cell fusion was monitored by cell–cell content mixing or cell–cell lipid mixing after co-incubation of effector cells (Env-transfected 293T cells) with target cells (3T3.CD4.CCR5). To express WT or AA mutant Env protein, we transfected 293T cells with Env-expression plasmids using Fugene HD (Roche Diagnostics) at 3:1 ratio (v/w). Thirty-six hours after the transfection, 293T

Fig. 7. MPER conformation change during HIV membrane fusion. (a) Illustrations of the HIV fusion process following CD4 binding. Chemokine receptors are omitted at the pre-fusion stage and only one gp41 monomer is drawn in the intermediate stages for simplicity. MPER is highlighted in red. (b) Hinge conformation revealed by backbone dihedral angles for free and BNAb-bound HxB2 WT MPER derived from observed NMR chemical shifts, except for 10E8 where the angles are extracted from a crystal structure (PDB ID: 4G6F). The backbone dihedral angles extracted from unbound Con089 and HxB2-AA peptide NMR structures are shown for comparison. (c) Side-chain oxygen (green) to backbone amide (blue) hydrogen bonds observed in crystal structures of MPER bound to BNAbs: (top) between N671 and D674 in 10E8, (middle) between N671 and F673 in 4E10 (PDB ID: 2FX7) and (bottom) between D674 and T676 in Z13e1 (PDB ID: 3FN0). (d) Orientation change of W672/F673 with respect to the membrane with different N-capping of the C-terminal helix in 10E8-bound and unbound MPER.

cells were detached and stained with gp120-specific anti-V3 loop antibody 1A3 to determine the expression level. The amounts of Env-expressing plasmids were adjusted to yield comparable expression levels of WT Env protein and AA mutant Env protein on the surface of 293T cells.

Luciferase reporter assay of cell-to-cell fusion

To quantitatively analyze Env-mediated cell–cell fusion process, we used TZM-bl cells, which contain Tat-responsive reporter genes for firefly luciferase, as target cells. 293T cells transfected with Env-expressing plasmids together with Tat-expressing plasmids were mixed with TZM-bl cells at 1:1 ratio. Cell mixtures were cultured in 96-well plates in triplicates with 20,000 cells in each well. At various time points, cultured cells were taken out and stored at −80 °C. After the final collection, cells were lysed and the luciferase activity was measured using Steady-Glo Luciferase assay system (Promega).

Cytoplasmic dye transfer assays

Effector cells were loaded with cytoplasmic dye Calcein-AM at a concentration of 0.5 μM, and target cells were loaded with cytoplasmic dye CMTMR (Invitrogen, Grand Island, NY) at a concentration of 10 μM for 30 min at 37 °C. After washing three times with phosphate-buffered saline, we mixed the two cell populations at 1:1 ratio and cultured 300,000 cells in a 24-well plate. Images of cells were taken using Nikon eclipse Ti fluorescence microscope after co-incubation for 4 h or overnight.

Lipid mixing assays

The cell–cell lipid mixing was performed similar to the cell–cell content mixing, except that effector cells and target cells were stained with lipophilic dyes DiO (Invitrogen) and DiI (Invitrogen), respectively, and images were acquired 2 h after co-incubation. Fusion defective Env-transfected 293T effector cells were compared as a negative control. All experiments were repeated three times, and representative images were shown.

Flow cytometric analysis of efficiency of membrane lipid transfer during fusion

293T cells transfected with either Env WT or AA mutant-expressing plasmids or empty plasmids were stained with lipophilic dye DiO while TZM-bl cells were stained with lipophilic dye DiD. We cultured 300,000 of mixed cells at 1:1 ratio in a 24-well plate for 2 h at 37 °C, dissociated with phosphate-buffered saline and 25 mM ethylenediaminetetraacetic acid (EDTA), washed and immediately subjected to flow cytometric analysis. DiO and DiD double positive population comprises cells with fused membrane. The percentage of fused double positive cells were calculated to quantify hemifusion efficiency of WT and AA mutant following the subtraction of background dye redistribution between empty vector-transfected effector and target cells, and the lipid mixing activity for AA mutant was normalized to that of WT in three independent experiments, averaged and plotted.

EPR measurements

EPR power saturation measurements were performed on a Bruker EMX spectrometer using a loop-gap resonator. The immersion depths values were calculated by the ratio of accessibility value of O_2 to 50 mM nickel (II) ethylenediaminediacetic acid. Samples were purged by either a stream of air or nitrogen gas. EPR distance measurements were performed with a Bruker ELEXSYS E680 spectrometer using two EPR techniques: conventional EPR (used for preliminary assessment) and pulsed EPR (sensitive distance range, 15–80 Å). Pulsed EPR DEER experiments were carried out using a dead-time-free pulse sequence as described previously [29]. Conventional EPR and DEER spectra were analyzed with a Monte Carlo/Simplex Gaussian convolution method to extract spin–spin distance [30].

NMR structure determination

NMR experiments were performed using Bruker, Agilent spectrometers equipped with cryogenic probes operating at ^{1}H frequency between 900 and 600 MHz at 35 °C, using typically 1 mM isotopically labeled MPER samples in 90% H_2O/10% D_2O, pH adjusted to 6.6, with 100 mM d38-DPC. NMR structural determination of HxB2-AA mutant was carried out at a lower peptide concentration (500 μM) to prevent aggregation. Two-dimensional and ^{15}N or ^{13}C edited three-dimensional nuclear Overhauser enhancement (NOE) spectroscopy data sets are collected with 60 ms mixing time. RDC data from JNH by transverse relaxation optimized spectroscopy experiment, and CAHA [31], JNCO [32] and JCOCA [33] by quantitative J experiments were collected using aligned samples containing 1 mM MPER and 20 mg/ml DNA nanotube material. Weakly oriented HDO with ~20 mg/ml DNA yielded ^{2}H quadrupolar splitting of 7–8 Hz in 500 MHz magnet field.

NMR data were processed by NMRPipe [34]. NMR resonance and NOE assignments were completed using CARA [35]. NOE distances were calibrated using CYANA [36]. Backbone dihedral angles restraints are derived from HNHA experiment and chemical-shift-based TALOS+ program [37] that are consistent with local NOE restraints. EPR membrane immersion data were adopted after taking into account the maximum length (7 Å) and dynamics of the nitroxide spin-label used in the EPR experiments. Structure models were calculated using Xplor-NIH [38] software with a TENSO module [39] incorporating RDC restraints during high-temperature torsion angle dynamics stage and planeDisPot module [40] incorporating EPR depth restraints during subsequent low-temperature Cartesian coordinate dynamics stage.

DNA nanotube production

The modified p7308-bases-long M13mp18 phage DNA was generated at the nanomole scale as described previously [41,42]. DNA staple oligonucleotide strands were prepared by solid-phase chemical synthesis

(Invitrogen) on the 200-nmol scale in salt-free purification grade and dried format. Each monomer folding mixture was prepared by combining 120 nM phage DNA and 720 nM DNA staple in a pH 8.0 buffer (5 mM Tris Cl, 1 mM EDTA, pH 8.0, 20 mM $MgCl_2$), aliquoted into four 96-well plates with 150 µl per well (36 ml each monomer). The folding ramp was as follows: 80 °C for 5 min, decrease by 1°/5 min to 65 °C and then decrease by 1°/40 min to 20 °C. Each folded monomer sample was pooled and purified separately from excess staple strands via gravity-flow ion-exchange chromatography (Qiagen-Tip 10000 Column), as described previously [17]. Nanotube heterodimers were self-assembled by combining purified front and rear monomer mixtures together and incubated at 37 °C for 2 h and then precipitated by addition of 0.25 volumes of 20% polyethylene glycol 8000 followed by incubation at room temperature for 15 min. The nanotubes were recovered by centrifugation at 15,000*g* for 30 min at 4 °C, resuspended in 2.5 mM Tris, 0.5 mM EDTA (pH 8.0) and 10 mM $MgCl_2$, then concentrated to 30 mg/ml and buffer-exchanged into desired protein buffer (90% H_2O/10% D_2O, 5 mM $MgCl_2$, 5 mM $NaPO_4$, pH 6.6) with Centricon-100. Finally, 260 µl of 20 mg/ml nanotubes was mixed with 260 µl of 1 mM $^{15}N/^{13}C$-labeled MPER sample containing 100 mM d38-DPC and 50 mM NaCl before concentrated down to 260 µl using a Centricon-3 concentrator.

Accession numbers

The structure coordinates and NMR restraints have been deposited with Protein Data Bank (PDB ID: 2ME1, 2ME2, 2ME3, 2ME4) and Biological Magnetic Resonance Bank (BMRB ID: 19515, 19513, 19514, 19515) databases.

Acknowledgements

This work is funded by National Institutes of Health Grants AI084785 and AI091693 to E.L.R., GM047467 to G.W. and 1DP2OD004641 and 1U54GM094608 to W.S., as well as Gates Foundation Grants to E.L.R. and M.S.S. Y.C. is affiliated with the PhD Program in Biological Sciences in Public Health at Harvard School of Public Health, Boston, MA, USA. L.S. acknowledges the support of National High Magnetic Field Laboratory User Collaboration Grants Program Grant No. 5080. The National High Magnetic Field Laboratory is funded by National Science Foundation Cooperative Agreement No. DMR1157490, Department of Energy and the State of Florida. We thank Drs. J. G. Sodroski, B. Haynes, R. Swanstrom and R. T. Wyatt for reagents; Drs. J. Chou and M. Allan for advice with RDC data; J. -H. Wang for comments; and G. Heffron for assistance with NMR instruments.

Received 26 July 2013;
Received in revised form 18 September 2013;
Accepted 20 September 2013

Available online 26 September 2013

Keywords:
viral membrane fusion;
NMR solution structure;
helix–hinge–helix motif;
helix capping;
broadly neutralizing antibody

Present address: U. J. Kudahl, Technical University of Denmark, 2800 Lyngby, Denmark.
Present address: L. Yu, University of Science and Technology of China, Hefei 230031, China.
Present address: G. Bellot, Institut de Génomique Fonctionnelle, CNRS UMR 5203, INSERM U661, F-34000 Montpellier, France.

Abbreviations used:
BNAb, broadly neutralizing antibody; DPC, dodecylphosphocholine; DEER, double electron–electron resonance; EDTA, ethylenediaminetetraacetic acid; MPER, membrane proximal external region; NOE, nuclear Overhauser enhancement; RDC, residual dipolar coupling; WT, wild type.

References

[1] Harrison SC. Viral membrane fusion. Nat Struct Mol Biol 2008;15:690–8.
[2] Roux KH, Taylor KA. AIDS virus envelope spike structure. Curr Opin Struct Biol 2007;17:244–52.
[3] Chan DC, Fass D, Berger JM, Kim PS. Core structure of gp41 from the HIV envelope glycoprotein. Cell 1997;89:263–73.
[4] Weissenhorn W, Dessen A, Harrison SC, Skehel JJ, Wiley DC. Atomic structure of the ectodomain from HIV-1 gp41. Nature 1997;387:426–30.
[5] Tan K, Liu J, Wang J, Shen S, Lu M. Atomic structure of a thermostable subdomain of HIV-1 gp41. Proc Natl Acad Sci USA 1997;94:12303–8.
[6] Chojnacki J, Staudt T, Glass B, Bingen P, Engelhardt J, Anders M, et al. Maturation-dependent HIV-1 surface protein redistribution revealed by fluorescence nanoscopy. Science 2012;338:524–8.
[7] Ivankin A, Apellániz B, Gidalevitz D, Nieva JL. Mechanism of membrane perturbation by the HIV-1 gp41 membrane-proximal external region and its modulation by cholesterol. Biochim Biophys Acta 2012;1818:2521–8.
[8] Vishwanathan SA, Hunter E. Importance of the membrane-perturbing properties of the membrane-proximal external region of human immunodeficiency virus type 1 gp41 to viral fusion. J Virol 2008;82:5118–26.
[9] Muñoz-Barroso I, Salzwedel K, Hunter E, Blumenthal R. Role of the membrane-proximal domain in the initial stages of human immunodeficiency virus type 1 envelope glycoprotein-mediated membrane fusion. J Virol 1999;73:6089–92.
[10] Salzwedel K, West JT, Hunter E. A conserved tryptophan-rich motif in the membrane-proximal region of the human immunodeficiency virus type 1 gp41 ectodomain is important for Env-mediated fusion and virus infectivity. J Virol 1999;73:2469–80.

[11] Sun ZY, Oh KJ, Kim M, Yu J, Brusic V, Song L, et al. HIV-1 broadly neutralizing antibody extracts its epitope from a kinked gp41 ectodomain region on the viral membrane. Immunity 2008;28:52–63.
[12] Cardoso RM, Zwick MB, Stanfield RL, Kunert R, Binley JM, Katinger H, et al. Broadly neutralizing anti-HIV antibody 4E10 recognizes a helical conformation of a highly conserved fusion-associated motif in gp41. Immunity 2005;22:163–73.
[13] Huang J, Ofek G, Laub L, Louder MK, Doria-Rose NA, Longo NS, et al. Broad and potent neutralization of HIV-1 by a gp41-specific human antibody. Nature 2012;491:406–12.
[14] Nelson J, Brunel FM, Jensen R, Crooks ET, Cardoso RM, Wang M, et al. An affinity-enhanced neutralizing antibody against the membrane-proximal external region of human immunodeficiency virus type 1 gp41 recognizes an epitope between those of 2F5 and 4E10. J Virol 2007;81:4033–43.
[15] Kudahl U, Simon C, Zhang G, Reinherz EL, Brusic V. Motiffinder. http://research4.dfci.harvard.edu/cvc/motiffinder/; 2012.
[16] Haim H, Strack B, Kassa A, Madani N, Wang L, Courter JR, et al. Contribution of intrinsic reactivity of the HIV-1 envelope glycoproteins to CD4-independent infection and global inhibitor sensitivity. PLoS Pathog 2011;6:e1002101.
[17] Douglas SM, Chou JJ, Shih WM. DNA-nanotube-induced alignment of membrane proteins for NMR structure determination. Proc Natl Acad Sci USA 2007;104:6644–8.
[18] Buzon V, Natrajan G, Schibli D, Campelo F, Kozlov MM, Weissenhorn W. Crystal structure of HIV-1 gp41 including both fusion peptide and membrane proximal external regions. PLoS Pathog 2010;6:e1000880.
[19] Doig AJ, Baldwin RL. N- and C-capping preferences for all 20 amino acids in alpha-helical peptides. Protein Sci 1995;4:1325–36.
[20] Richardson JS, Richardson DC. Amino acid preferences for specific locations at the ends of alpha helices. Science 1988;240:1648–52.
[21] Ofek G, Tang M, Sambor A, Katinger H, Mascola JR, Wyatt R, et al. Structure and mechanistic analysis of the anti-human immunodeficiency virus type 1 antibody 2F5 in complex with its gp41 epitope. J Virol 2004;78:10724–37.
[22] Julien JP, Bryson S, Nieva JL, Pai EF. Structural details of HIV-1 recognition by the broadly neutralizing monoclonal antibody 2F5: epitope conformation, antigen-recognition loop mobility, and anion-binding site. J Mol Biol 2008;384:377–92.
[23] Kim M, Sun ZY, Rand KD, Shi X, Song L, Cheng Y, et al. Antibody mechanics on a membrane-bound HIV segment essential for GP41-targeted viral neutralization. Nat Struct Mol Biol 2011;18:1235–43.
[24] Song L, Sun ZY, Coleman KE, Zwick MB, Gach JS, Wang JH, et al. Broadly neutralizing anti-HIV-1 antibodies disrupt a hinge-related function of gp41 at the membrane interface. Proc Natl Acad Sci USA 2009;106:9057–62.
[25] Kumauch IM, Kaledhonkar S, Philip AF, Wycoff J, Hara M, Li Y, et al. A conserved helical capping hydrogen bond in PAS domains controls signaling kinetics in the superfamily prototype photoactive yellow protein. J Am Chem Soc 2010;132:15820–30.
[26] Yu S, Maillard RA, Gribenko AV, Lee JC. The N-terminal capping propensities of the D-helix modulate the allosteric activation of the *Escherichia coli* cAMP receptor protein. J Biol Chem 2012;287:39402–11.
[27] Bailey GD, Hyun JK, Mitra AK, Kingston RL. A structural model for the generation of continuous curvature on the surface of a retroviral capsid. J Mol Biol 2012;417:212–23.
[28] Pace CN, Scholtz JM. A helix propensity scale based on experimental studies of peptides and proteins. Biophys J 1998;75:422–7.
[29] Pannier M, Veit S, Godt A, Jeschke G, Spiess HW. Dead-time free measurement of dipole-dipole interactions between electron spins. J Magn Reson 2000;213:316–25.
[30] Sale K, Song L, Li Y, Perozo E, Fajer PG. Improvement of EPR distance measurements using molecular modeling of spin probes. J Am Chem Soc 2005;127:9334–5.
[31] Call ME, Schnell JR, Xu C, Lutz RA, Chou JJ, Wucherpfennig KW. The structure of the zetazeta transmembrane dimer reveals features essential for its assembly with the T cell receptor. Cell 2006;127:355–68.
[32] Chou JJ, Delaglio F, Bax A. Measurement of one-bond ^{15}N-$^{13}C'$ dipolar couplings in medium sized proteins. J Biomol NMR 2000;18:101–5.
[33] Jaroniec CP, Ulmer TS, Bax A. Quantitative J correlation methods for the accurate measurement of $^{13}C'$-^{13}Calpha dipolar couplings in proteins. J Biomol NMR 2004;30:181–94.
[34] Delaglio F, Grzesiek S, Vuister GW, Zhu G, Pfeifer J, Bax A. NMRPipe: a multidimensional spectral processing system based on UNIX pipes. J Biomol NMR 1995;6:277–93.
[35] Keller RLJ. Computer aided resonance assignment tutorial. Goldau, Switzerland: Cantina Verlag; 2004.
[36] Güntert P, Mumenthaler C, Wüthrich K. Torsion angle dynamics for NMR structure calculation with the new program DYANA. J Mol Biol 1997;273:283–98.
[37] Shen Y, Delaglio F, Cornilescu G, Bax A. TALOS+: a hybrid method for predicting protein backbone torsion angles from NMR chemical shifts. J Biomol NMR 2009;44:213–23.
[38] Schwieters CD, Kuszewski JJ, Tjandra N, Clore GM. The Xplor-NIH NMR molecular structure determination package. J Magn Reson 2003;160:65–73.
[39] Sass HJ, Musco G, Stahl SJ, Wingfield PT, Grzesiek S. An easy way to include weak alignment constraints into NMR structure calculations. J Biomol NMR 2001;21:275–80.
[40] Xu C, Gagnon E, Call ME, Schnell JR, Schwieters CD, Carman CV, et al. Regulation of T cell receptor activation by dynamic membrane binding of the CD3epsilon cytoplasmic tyrosine-based motif. Cell 2008;135:702–13.
[41] Berardi MJ, Shih WM, Harrison SC, Chou JJ. Mitochondrial uncoupling protein 2 structure determined by NMR molecular fragment searching. Nature 2011;476:109–13.
[42] Douglas SM, Dietz H, Liedl T, Högberg B, Graf F, Shih WM. Self-assembly of DNA into nanoscale three-dimensional shapes. Nature 2009;459:414–8.